Indian Journal of Biochemistry & Biophysics
Vol. 63, April 2026, pp. 453-468
DOI: 10.56042/ijbb.v63i4.22123

The effect of exothermic reaction associated with activation energy in hydromagnetic convection heat transfer flow of Water based ($MoS_2 – SiO_2$ / H_2O) hybrid nanofluid through a cylindrical annulus with variable viscosity: Darcy-forchheimer model

Janapati Siva Shankara Rao[1]*, Kakarla Sree Ranga Vani[2] & Juturu Sathyamaiah Sukanya[3]

[1]Department of Mathematics, Government College (A), Anantapur -515 001, Andhra Pradesh, India

[2]Department of Mathematics and Computer Science, Sri Satya Sai Institute of Higher Learning, Anantapur-515 001, Andhra Pradesh, India

[3]Department of Mathematics, Srinivasa Ramanunan Institute of Technology (Autonomous), Ananthapuramu-515 701, Andhra Pradesh, India

Received 28 July 2025; *revised 11 November 2025*

The growing need for effective thermal management in industrial processes, renewable energy systems, and advanced cooling technologies has intensified the search for high-performance heat transfer fluids. Hybrid nanofluids, formed by combining different nanoparticles, present a promising approach as they significantly improve heat and mass transfer characteristics compared to conventional fluids. This article explores the effects of exothermic chemical reaction associated with activation energy, viscosity of variable in hydro-magnetic non-Darcy convection heat transfer flow of water base (MoS_2+SiO_2) hybrid in cylindrical annulus. The governing non-linear together equations were executed by employing Galarkin's finite-element method with QIF (Quadratic Interpolation Functions) and u (velocity), θ (temperature) and C (nano-concentration) profiles be demonstrated graphically. It is found that rate of heat transfer (Nu) grows at inner cylinder and decays at outer cylinder with the decreasing values of ϕ/ Ec/ B/ E_1 in both nanofluids. An uplift in reaction rate (Q_1) reduces (τ,Nu and Sh) in hybrid and increases in mono nanofluids at both the cylinders. The variations of Nu and Sh for different parameters show that Nu and Sh in hybrid-nanofluid are relatively greater than those in mono nanofluid. These findings yield important insights for optimization of thermal systems, contributing to enhanced energy efficiency and reduced operational costs across diverse engineering applications

Keywords: Dissipative energy, Heat transfer, Non-uniform heat sources, Nusselt number, Porous medium, Sherwood number, Thermal radiation

Nanoparticles are made from many different materials, including metallic oxides (Al_2O_3, CuO), Molybdenum sulphide (MoS_2), and Silicon oxide (SiO_2). They can also be made from nitride ceramics (AlN, SiN), carbide ceramics (SiC, TiC), metals (Cu, Ag, Au), semiconductors (TiO_3, SiC), and more. When they are mixed with base fluids, they have big effects on how well heat moves. Nanofluids are very useful in some technical fields, like cooling electronics and vehicles; in biomedicine, like killing cancer cells and saving lives during surgery; and in process industries, like making paper, chemicals, textiles, detergents, and foods and drinks. Choi and Jeffrey[1] recently discovered nanofluids, which are made up of nanoparticles (<100nm) that are mixed in with base fluids like water, oil, and ethylene glycol. The nano layer works as a thermal bridge between the solid nanoparticle and the base fluid. If nanofluids have nanoparticles in them, Brownian diffusion and heat movement can happen. So, nanofluids are heat transfer fluids that conduct heat very well. They make big heat exchangers used in chemical plants and smaller heat exchangers used in cars work better. According to Nura Mu'az Muhammad and Nor Azwadi Che Sidik[2], Hasan *et al.*[3], Jing Liu and Zhong-Shan Deng[4] have talked about how nanofluids are used to cool factories because they are better at transferring heat, which saves energy. A number of researchers, including Yaseen *et al.*[5], Mishra *et al.*[6], and Iqbal *et al.*[7], have shown that a hybrid nanofluid (MoS_2–SiO_2/water, MoS_2-SiO_2/H_2O, and MoS_2-SiO_2–GO/H_2O) can flow with viscous dissipation and Ohmic heating on an irregular, variable-thick, convex

*Correspondence:
E-mail: sankarj07@gmail.com

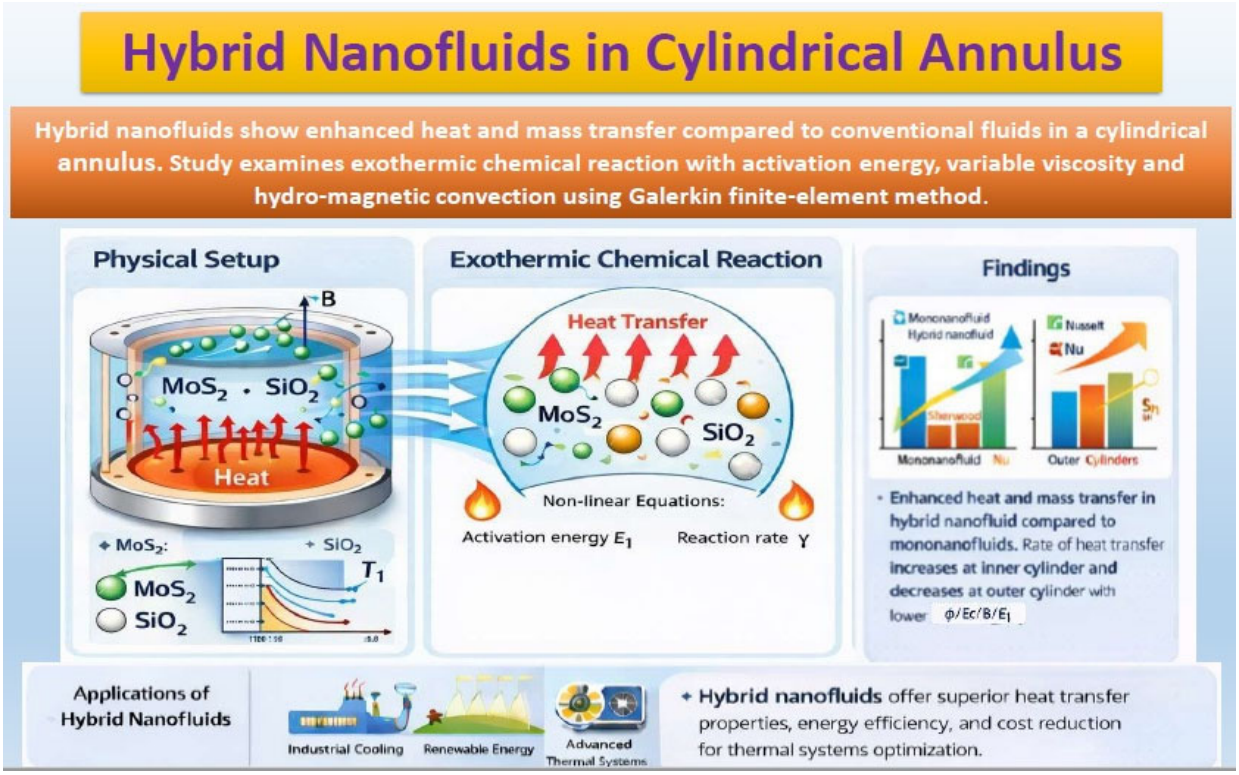

Graphical abstract

or concave-shaped sheet in a porous medium, as well as generate and absorb heat.

Recent scientific and industrial advances in cylinder fluid flow and heat transfer have increased their relevance. Optical fibre coating, nanowire manufacture, cancer therapy, metal spinning, and industrial manufacturing use it. Cylinder fluid flow was studied by various academics[8,9]. Heat transmission and entropy formation of turbulent flow between concentric cylinders were studied by Liu *et al.*[10]. Adding mono and hybrid nanoparticles to hybrid nanofluid flow among (two) concentric cylinders boosted heat transmission by 10.1% and 11.3%, respectively, according to Hanif *et al.*[11]. Iron oxide affected magnetised fluid flow heat transfer and entropy formation in coaxial cylindrical shape, according to Sun *et al*[12]. As Hartman number climbed from 0 to 186, fractional entropy generation increased by 21.72% but thermal entropy dropped by 17.15%. Impulsively moving ternary nanofluid over a rough-yawed cylinder was explored by Patil *et al*[8]. Heat transport and flow of CuO-Ag/water/ethylene glycol between two coaxial cylinders were numerically studied by Zangooee *et al*[13]. Magnetic field and Joule heating boost hybrid nanofluid heat transfer, according to their study. The investigation shows that strengthening a magnetic field reduces vortex disintegration. Hafez[14] studied Sisko fluid peristalsis time-dependent flow between two cylinders in an electric field. Swamy *et al.*[15], Mahfoud[16], Hanif *et al.*[17] addressed hybrid nanofluid flow between two coaxial cylinders' heat transfer. MHD convective-based SWCNT-MWCNT-GO ternary hybrid nanofluids with variable viscosity and exothermic reactions were investigated by Chandrakala and Rao[18].

A chemical reaction changes the amount and composition of its constituent parts. Disruption of the chemical bond between atoms results in the transmission of just their interior structures. One of the most crucial variables affecting the velocity of a chemical reaction is the nature of the reaction itself. To improve conventional fluid heat transmission, the chemical reaction is crucial. Using mass and heat transfer resulting from chemical reactions, significant engineering tasks like drying, temperature, and moisture distribution can be accomplished in the industrial business. The concentration of the reactant determines the response rate in the majority of chemical reaction instances. When the rate of reaction is proportional to the concentration of the reactant, we say that there has been a chemical reaction. Exothermic and endothermic reactions are the two main categories

of chemical processes. When a process releases heat yet modifies enthalpy in a negative way, we say that it is an exothermic reaction. But, as a consequence, many chemical reactions release either heat, light, or sound. Food processing, chemical engineering, oil emulsions, and geothermal reservoirs are some of the significant areas that benefit from the chemical reaction and activation energy. For chemical reactions involving MHD convection and a finite Arrhenius activation energy, Krishna *et al*.[19] investigated the hall effects. Netai Roy and Dulal Pal[20] looked at how a Casson nanofluid's heat and mass transfer over a stretching sheet is affected by factors such activation energy, radiation, nonlinear thermal radiation, and ohmic dissipation. Using a spectral collocation approach, Obalalu *et al*.[21-23] and Electrical conductivity affects the thermal stability of MHD reactive compressed fluid flow through a channel when Arrhenius energy and exothermic chemical reactions occur, according to Adeshina *et al*.[24].

The essential physical characteristics of a fluid, specifically viscosity, fluctuate with temperature and play a crucial role in the behaviour of nanofluids. The thermal energy produced by internal friction elevates the temperature, subsequently influencing the viscosity of the fluid. Therefore, the viscosity of fluids should not be regarded as a constant value. Therefore, it is imperative to consider that viscosity is likely to vary with temperature. Accurate prediction of the heat transfer rate necessitates consideration of the temperature-dependent variation of viscosity. The fluctuation of viscosity within the thermal boundary layer is significant. This problem has numerous applications, including in the processes of hot rolling, wire drawing, glass fibre production, paper manufacturing, the adhesion of labels to hot surfaces, the drawing of plastic films, and the examination of pollutant crude oil spills on seawater surfaces. A multitude of researchers have examined the influence of MHD, thermal radiation, the Hall effect, and temperature-dependent viscosity on the heat and mass transfer characteristics of laminar boundary layer flow involving Al_2O_3-ethylene glycol nanofluid over a stretching sheet, as discussed by various authors including Chitti Babu[25], and Sreedevi *et al*.[26]. Further, the discourse on Nagasasikala[27] addressed the implications of exothermic reactions linked to activation energy on the magnetohydrodynamic rotating convective heat and mass transfer flow of Water/Eg/Eo based TiO_2 nanofluid over a stretching surface with variable viscosity.

Darcy's law is a basic rule that shows how pressure drop and speed are related when fluids run through porous materials. Henry Darcy first came up with it after experimenting with how water moves through sand beds. It is often used to Figure out how water moves through aquifers and how gas, water, and oil move through oilfield reservoirs. Darcy's linear model doesn't work well with higher flow rates, though, because it doesn't take into account the effects of inertia. In order to get around this problem, an extra term is added: the Forchheimer adjustment. Researchers led by Forchheimer[28] looked at how fluid moved through porous media at high speeds and saw that as the flow rate went up, inertial forces started to have a big effect on the movement of the fluid. He recommended adding a term for the fluid's kinetic energy to Darcy's equation so that these effects could be taken into account. The Darcy-Forchheimer model is one of the most common ways to explain nonlinear flow patterns in porous media. It is an extension of Darcy's law. Researchers like Wooding[29] and Brinkman[30,31] have made more changes to Darcy's formula over time to make it a better picture of convective flow in porous structures.

Using nanoparticles in a porous material seems to be a great way to improve the properties of convection heat transfer for manufacturing processes these days. Because of this, porous media technology interested a lot of experts who wanted to learn more about how it could be used with other kinds of fluids and mixtures. Using this method has already led to many changes in industry, such as underground water sources, better insulation, better oil production, and a wide range of heating systems. Many studies look at the thermo-physical properties and heat transfer qualities of Molybdenum sulphide (MoS_2) and silicon oxide (SiO_2)/water hybrid nanofluids. Some studies also look at how the shape of the nanoparticles and other factors affect the flow and heat transfer. These studies don't directly look at "exothermic reactions" in the nanofluid, but they do look at how heat creation and other things affect the behaviour of the nanofluid. MoS_2+SiO_2/water hybrid nanofluid focuses on their thermophysical properties and how they transfer heat. Researchers are looking into how the shape of the nanoparticles and different factors affect the flow of the fluid and the transfer of heat. Aamir Ali *et al*.[32] have studied thermal analysis of MHD radiative flow of hybrid nanofluids in a porous medium between coaxial

cylinders. They revealed that increasing the magnetic field strength reduces the fluid velocity, indicating strong magnetic damping effects.

This work investigates the behaviour of a water-based hybrid (MoS_2+SiO_2) nanofluid in a cylindrical annulus with a spatially changing heat source or sink. Molybdenum disulphide (MoS_2), a metal dichalcogenide, has alternating molybdenum and sulphur layers. Molybdenite, a black-silver crystal mineral, occurs naturally. High temperatures and low interfacial energy make it an effective nanofluid stabiliser. Unlike molybdenum, silicon dioxide (SiO_2) inhibits sulfatase formation due to its higher electronegativity. Considering these material features, we study the flow dynamics of an inflexible, laminar water-based hybrid nanofluid with MoS_2 and SiO_2 particles in a cylindrical annular shape.

Applications

Transport phenomena affected by thermal and concentration buoyancy are essential in numerous engineering systems and natural habitats. These processes are extensively employed in sectors like chemical distillation, heat exchangers, solar energy collection, and thermal protection systems, where the impetus originates from the synergistic effects of heat and chemical reactions. In atmospheric flows, thermal convection caused by sunlight is affected by fluctuations in water vapour concentration. Buoyancy-driven convection arising from the interplay of heat and mass transmission in porous media has substantial applications in energy engineering. These encompass moisture migration, fibre insulation, and chemical pollutant dispersion in saturated soils, geothermal energy extraction, and subterranean disposal of hazardous waste. This study on flow and heat transmission between concentric cylinders is very pertinent to nuclear waste disposal studies. Radioactive waste can be safely stored underground to reduce human exposure. The scientific and industrial progress in fluid dynamics and thermal transfer within cylindrical structures has highlighted their significance. Applications encompass optical fibre coating, nanowire production, cancer treatment, metal spinning, and numerous other industrial manufacturing techniques. Figure 1b showcases different of nanofluids applications.

Novelty

This study presents a unique investigation into the flow dynamics of magneto-radiative water-based hybrid nanofluids (MoS_2 + SiO_2) within a concentric annulus. It meticulously considers factors such as viscous dissipation, thermal radiation, Joule heating, exothermic reactions, thermos-diffusion, activation energy, non-Darcy effects, and the influence of non-uniform heat sources and sinks on convective heat and mass transfer processes.

Formulation of the Problem

This research examines the complex interplay of mixed convective flow involving water-based hybrid nanofluids (MoS_2 + SiO_2) as they traverse a porous medium situated within a vertical circular annulus, under conditions of constant concentration and thermal maintenance. The Boussinesq approximation is employed to address density variations that are confined to thermal and molecular buoyancy forces. The momentum equation in the porous region is written using the Brinkman-Forchheimer-Extended Darcy model, which takes into account the effects of inertia and surface interactions. The governing equations are nonlinear and coupled, but the flow of fluid is only going in one way along the axial path of the cylinder annulus.

The subsequent assumptions underpin the flow problem.

- The flow exhibits characteristics of linearity and steadiness.
- Implementing the Boussinesq approximation to address density variations constrained to thermal and molecular buoyancy forces.
- In the context of a small magnetic Reynolds number, one can disregard the induced magnetic field when juxtaposed with the applied magnetic field.
- The surfaces of the cylinders are enveloped in a porous medium, with the separation between them measured as b-a. At r=a, the inner cylinder is maintained at a temperature T_i and a concentration C_t, whereas the outer cylinder, located at r=b, is kept at a temperature T_0 and a concentration C_0.
- The direction of flow is orientated vertically upward. Z-axis.
- Under the assumption of infinitely long cylinders, the flow and thermal characteristics of the fluids are regarded as fully developed.
- The energy equation integrates constraints related to non-uniform heat sources and sinks.
- The effects of viscosity and Joule heating are duly considered.

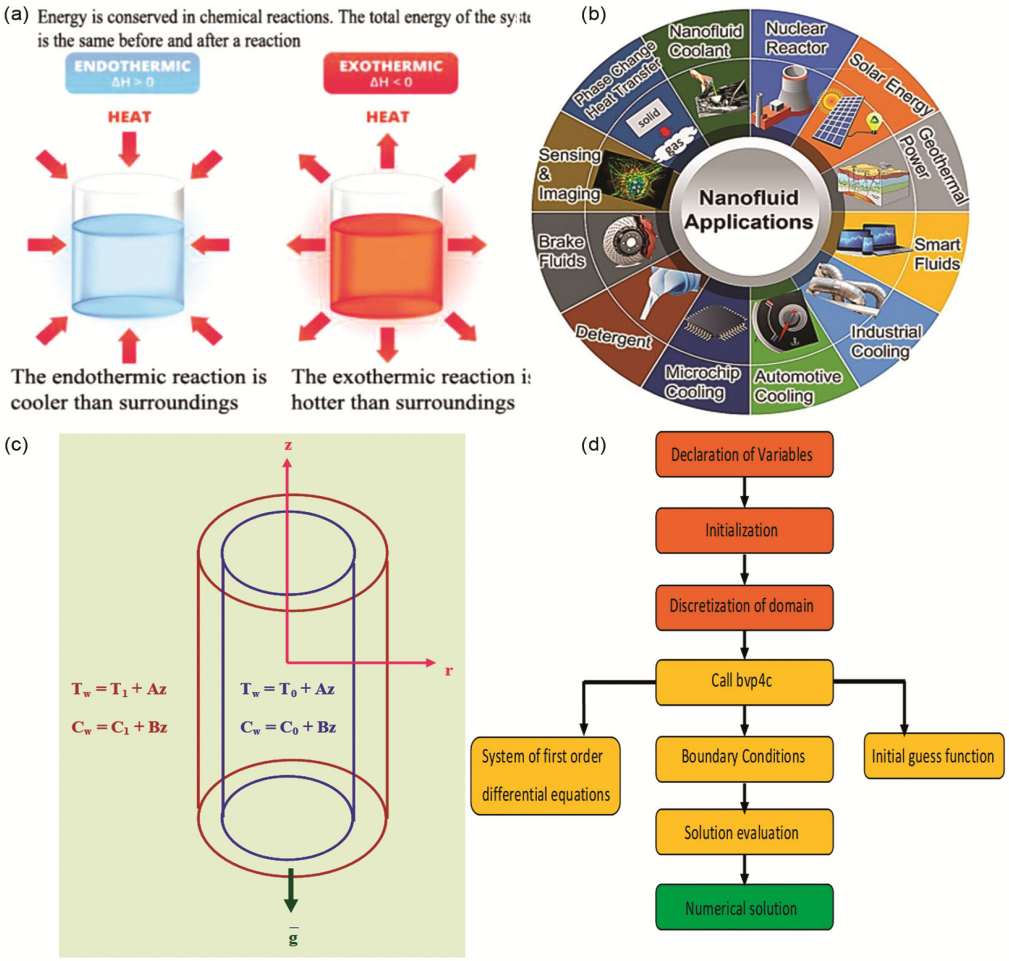

Fig. 1 — (a) Chemical reactions with exothermic and endothermic; (b) Various applications associated with nanofluids; (c) ConFigureureuration of the flow geometry; and (d) BVP4c flow chart

❖ The implications of the Darcy-Forchheimer phenomena are also taken into account for the flow system.

Assuming the aforementioned, the governing equations[33] are

$$-\frac{\partial p}{\partial z}+\frac{1}{\rho_{hnf}\delta_1 r}\frac{\partial}{\partial r}\left((\mu_{hnf}(T)\,\mathrm{r}\frac{\partial u}{\partial r})\right)-(\frac{\mu_{hnf}}{\rho_{hnf}k})u$$
$$-\frac{\sigma_f(T)\mu_e^2 H_0^2}{\rho_{hnf}r^2}-\frac{\delta_1 F}{\rho_{hnf}\sqrt{k}}u^2 \qquad \ldots (1)$$
$$+(\rho\beta)_{hnf}(T-T_o)=0$$

$$(\rho C_p)_{hnf}u\frac{\partial T}{\partial z}=k_{hnf}(\frac{\partial^2 T}{\partial r^2}+\frac{1}{r}\frac{\partial T}{\partial r})+q'''$$
$$-\frac{1}{r}\frac{\partial(rq_r)}{\partial r}+\mu_{hnf}(\frac{du}{dr})^2+(\sigma_{hnf}\mu_e^2 H_o^2)(u^2) \qquad \ldots (2)$$
$$+Q_1'\,\mathrm{A}(C-C_0)(\frac{T}{T_o})^n Exp(-\frac{E_a}{KT})$$

$$u\frac{\partial C}{\partial z}=D_B\left(\frac{\partial^2 C}{\partial r^2}+\frac{1}{r}\frac{\partial C}{\partial r}\right)+\frac{D_m K_T}{T_s}\left(\frac{\partial^2 T}{\partial r^2}+\frac{1}{r}\frac{\partial T}{\partial r}\right)$$
$$-A(\mathrm{C}-\mathrm{C}_0)(\frac{T}{T_o})^n Exp(-\frac{E_a}{KT}) \qquad \ldots (3)$$

The relevant boundary conditions for the problem under consideration are as follows:

$$u=0,\quad T=T_i,\qquad C=C_i \quad on\ r=a,$$
$$u=0,\quad T=T_o,\qquad C=C_o \quad on\ r=a+s \qquad \ldots (4)$$

When a radial magnetic field is present, velocity is determined by the radial coordinate, whereas all other parameters, save, θ, C, and pressure, are determined by r and z, where z is the vertical. We take $\frac{dT}{dz}=A,\frac{dC}{dz}=B$ where A and B are Temperature and concentration gradients.

Non-dimensional variables are distinct

$$\eta^* = \frac{\gamma}{a}, z^* = \frac{z}{a}, s^* = \frac{s}{a}, p^* = \frac{pa^2\delta_1}{\rho\nu_f^2}, \pi = \frac{dp^*}{dz},$$

$$u^* = \left(\frac{\nu_f}{a}\right)u,\ \theta = \frac{T - T_0}{T_i - T_0},\ C^* = \frac{C - C_0}{C_i - C_0}$$

The effective thermo-physical properties of hybrid and mono nanofluid are defined by Usman *et al*.[34]

Hybrid nanofluids

$$\mu_{hnf} = \frac{1}{\mu_f^{-1}(1-(\phi_1+\phi_2))^{2.5}}$$

$$(\rho Cp)_{hnf} = (1-(\phi_1+\phi_2))(\rho Cp)_f + \phi_1(\rho Cp)_{s1} + \phi_2(\rho Cp)_{s2}$$

$$\frac{k_{hnf}}{k_f} = \frac{\phi_1 k_1 + \phi_2 k_2 + 2(\phi_1+\phi_2)\mathrm{k}_f + 2(\phi_1+\phi_2)(\phi_1 \mathrm{k}_1 + \phi_2 \mathrm{k}_2) - 2(\phi_1+\phi_2)^2 k_f}{\phi_1 k_1 + \phi_2 k_2 + 2(\phi_1+\phi_2)\mathrm{k}_f - (\phi_1+\phi_2)(\phi_1 \mathrm{k}_1 + \phi_2 \mathrm{k}_2) + (\phi_1+\phi_2)^2 k_f}$$

$$\sigma_{hnf} = \frac{(1+2\phi_2)\sigma_{s2} + (1-2\phi_2)\sigma_{nf}}{(1-\phi_2)\sigma_{s2} + (1+\phi_2)\sigma_{nf}} \times \sigma_{nf}$$

Mono nanofluids

$$\mu_{nf} = \frac{1}{\mu_f^{-1}(1-(\phi_1))^{2.5}}$$

$$\rho_{nf} = (1-(\phi_1))\rho_f + \phi_1\rho_{s1}$$

$$(\rho Cp)_{nf} = (1-(\phi_1+))(\rho Cp)_f + \phi_1(\rho Cp)_{s1}$$

$$\rho_{hnf} = (1-(\phi_1+\phi_2))\rho_f + \phi_1\rho_{s1} + \phi_2\rho_{s2}$$

$$\frac{k_{nf}}{k_f} = \frac{\phi_1 k_1 + 2(\phi_1)\mathrm{k}_f + 2(\phi_1)(\phi_1 \mathrm{k}_1) - 2(\phi_1)^2 k_f}{\phi_1 k_1 + 2(\phi_1)\mathrm{k}_f - (\phi_1)(\phi_1 \mathrm{k}_1) + (\phi_1)^2 k_f}$$

$$\sigma_{nf} = \frac{(1+2\phi_1)\sigma_{s1} + (1-2\phi_1)\sigma_f}{(1-\phi_1)\sigma_{s1} + (1+\phi_1)\sigma_f} \times \sigma_f$$

The subscripts *hnf, nf, f*, and *s* indicate hybrid nanofluid, nanofluid, base fluid, and nanosolid particles each, whereas ϕ represents the solid volume fraction of the nanoparticles**.**

The following non-dimensional variables are defined for the analysis:

$$A_1 = \frac{1}{(1-\phi_1)^{2.5}(1-\phi_2)^{2.5}},$$

$$A_2 = (1-\phi_2)[(1-\phi_1) + \phi_1\frac{\rho_{s1}}{\rho_f}] + \phi_2\frac{\rho_{s2}}{\rho_f}$$

$$A_3 = (1-\phi_2)[(1-\phi_1) + \phi_1\frac{(\rho C_p)_{s1}}{(\rho C_p)_f}] + \phi_2\frac{(\rho C_p)_{s2}}{(\rho C_p)_f},$$

$$A_4 = (1-\phi_2)[(1-\phi_1) + \phi_1\frac{(\rho\beta)_{s1}}{(\rho\beta)_f}] + \phi_2\frac{(\rho\beta)_{s2}}{(\rho\beta)_f},$$

$$A_5 = \frac{k_{hnf}}{k_f},\ A_6 = \frac{\sigma_{hnf}}{\sigma_f}$$

The following table shows physical properties of water, MoS_2 and SiO_2. (Table 1).

The resulting non-dimensional equations are

$$\left.\begin{aligned}&(\frac{\partial^2 u}{\partial\eta^2} + \frac{1}{\eta}\frac{\partial u}{\partial\eta} - \mathrm{B}(\frac{\partial u}{\partial\eta})(\frac{\partial T}{\partial\eta})) = A_1A_3\,\mathrm{e}^{B\theta} + \delta_2A_1(D^{-1} + \frac{A_6M^2\,\mathrm{e}^{B\theta}}{\eta^2})u\\ &+\delta_2^{\,2}A_1(D^{-1})^{1/2}\Delta u^2 - \delta_2A_1A_4G\,\mathrm{e}^{B\theta}\,\theta\end{aligned}\right| \quad \text{... (5)}$$

$$\left.\begin{aligned}&(A_5 + \frac{4Rd}{3})(\frac{\partial^2\theta}{\partial\eta^2} + \frac{1}{\eta}\frac{\partial\theta}{\partial\eta}) + (A_{11}u + B_{11}\theta) + \mathrm{EcPr}(\mathrm{e}^{-B\theta})(\frac{du}{d\eta})^2\\ &+M^2Ec\,\mathrm{Pr}(u^2) + Q_1C(1+n\delta_1\theta)Exp(-\frac{E_1}{1+\delta_1\theta}) = A_3\,\mathrm{Pr}\,N_1u\end{aligned}\right| \quad \text{... (6)}$$

$$\left.\begin{aligned}&(\frac{\partial^2 C}{\partial\eta^2} + \frac{1}{\eta}\frac{\partial C}{\partial\eta}) = ScN_2\,u + ScSr\left(\frac{\partial^2\theta}{\partial\eta^2} + \frac{1}{\eta}\frac{\partial\theta}{\partial\eta}\right)\\ &-Q_1\gamma C(1+n\delta_1\theta)Exp(-\frac{E_1}{1+\delta_1\theta})\end{aligned}\right| \quad \text{... (7)}$$

where

$B = m\ (T_0 - T_i)$ (Viscosity parameter), $\Delta = FD^{-1/2}$ (Forchheimer number), $G = \frac{g\beta(T_e - T_i)a^3}{\nu^2}$ (Grashof number), $M^2 = \frac{\sigma\mu_e^2H_0^2}{a\nu}$ (magnetic parameter), $K = D^{-1} = \frac{a^2}{k}$ (Inverse Darcy parameter), $\mathrm{Pr} = \frac{\mu C_p}{k_f}$ (Prandtl number), $Rd = \frac{4\sigma^{\bullet}T_o^3}{k_f\beta_R}$ (Thermal radiation parameter), $Ec = \frac{\nu_f}{a^2C_p(T_i - T_0)}$ (Eckert number), $Sc = \frac{\nu}{D_B}$ (Schmidt number), $\gamma = \frac{k_T(\mathrm{T}_i - \mathrm{T}_o)a^2}{\mathrm{Q}_1^{'}(C_i - C_0)D_B}$

Table 1 — Physical properties (*Oztop and Abu-Nada*[35]).

Physical properties	Base fluid (water)	MoS_2	SiO_2
C_p(Jkg^{-1} K^{-1})	4179	397.21	703
ρ(kg m^{-3})	997.1	5060	2200
k(Wm^{-1} K^{-1})	0.612	904.4	1.2
βx10^{-5}k^{-1}	21.0	2.8424	0.056
σ (Sm^{-1})	5.5x10^{-4}	10^6	10^7

(Chemical Reaction parameter), $Sr = \frac{D_m K_T (T_0 - T_{i)}}{T_s (C_0 - C_i)}$

(Soret parameter), $Q_1 = \frac{Q_1^{'} \mathrm{A}(C_w - C_0)}{a^2 (T_w - T_0)\,\mathrm{k}_T}$ (Reaction rate parameter), $\theta_w = \frac{T}{T_o}$, $\delta_1 = \theta_w - 1$ (Temperature difference ratio), $E_1 = \frac{E_a}{KT_0}$ (Activation energy parameter). $A_{11} = \frac{A^*}{Av F}$ (Space dependent heat source), $B_{11} = \frac{B^*}{A^2 v F}$ (Temperature dependent heat source) and $N_1 = \frac{A}{a\Delta T}, N_2 = \frac{B}{a\Delta C}$.

The corresponding non-dimensional conditions are

$$\begin{aligned} &u = 0, \quad \theta = 1, \ C = 1 \quad on \quad \eta = 1 \\ &u = 0, \quad \theta = 0, \ \mathrm{C} = 0 \quad on \quad \eta = 1 + s \end{aligned} \qquad \ldots (8)$$

Finite element analysis

Finite elements with nonlinear quadratic estimate factors are studied across the circular duct's radial distance. θ, the behaviour of u, & C profiles is being digitally analysed for changes in regulating parameters. θIn finite element analysis, the Galerkin technique creates global linked indices for u, & C by variational formulation of each element, and C in e_k. θ_k, and Ck as residual values for u, θ, For an element e_k, assign u^k,

$$\left.\begin{aligned} E_u^k = {} & \frac{d}{d\eta}\left(\eta \frac{du^k}{d\eta}\right) - B\eta\left(\frac{du^k}{d\eta}\right)\left(\frac{d\theta^k}{d\eta}\right) + \delta_2 A_1 A_4 \eta G\, \mathrm{e}^{B\theta^k}(\theta^k) \\ & - \delta_2 A_1 \left(D^{-1} + \frac{A_6 M^2\, \mathrm{e}^{B\theta^k}}{\eta^2}\right)\eta u^k - A_1 \delta_2^{\,2} \Delta \eta (u^k)^2 - A_1 A_3\, \mathrm{e}^{B\theta^k} \end{aligned}\right| \qquad \ldots (9)$$

$$\left.\begin{aligned} E^k{}_\theta = {} & (\mathrm{A}_5 + \frac{4Rd}{3})\frac{1}{\eta}\frac{d}{d\eta}\left(\eta \frac{d\theta^k}{d\eta}\right) \\ & - A_5 P_r N_1 u^k + (A_{11} u^k + B_{11}\theta^k) \\ & + \mathrm{EcPr}(\mathrm{e}^{-B\theta^k})\left(\frac{du^k}{d\eta}\right)^2 + M^2 Ec\, \mathrm{Pr}(\mathrm{u}^k)^2 \\ & + Q_1 C^k (1 + n\delta_1\theta^k) Exp\left(-\frac{E_1}{1 + \delta_1\theta^k}\right) \end{aligned}\right| \qquad \ldots (10)$$

$$\left.\begin{aligned} E^k{}_c = {} & \frac{1}{\eta}\frac{d}{d\eta}\left(\eta \frac{dC^k}{d\eta}\right) - ScN_2 u^k - ScSr \frac{1}{\eta}\frac{d}{d\eta}\left(\eta \frac{d\theta^k}{d\eta}\right) \\ & - Q_1 \gamma C^k (1 + n\delta_1\theta^k) Exp\left(-\frac{E_1}{1 + \delta_1\theta^k}\right) \end{aligned}\right| \qquad \ldots (11)$$

where u^k, θ^k & C^k are arbitrary element of e_k and respective local nodal values as below.

$$u^k = u_1^k \psi_1^k + u_2^k \psi_1^k + u_3^k \psi_3^k,$$

$$\theta^k = \theta_1^k \psi_1^k + \theta_2^k \psi_2^k + \theta_3^k \psi_3^k, \quad C^k = C_1^k \psi_1^k + C_2^k \psi_2^k + C_3^k \psi_3^k$$

where ψ_1^k, ψ_2^k--------- *etc*. are Lagrange's quadratic polynomials.

We use Galarkin's method to turn the equations from (9) through (11) into a matrix equation structure, which gives us 3x3 local stiffness matrices. Adding the global nodal values and meeting the standards for inter-element continuity and equilibrium turns all the local matrices into a global matrix. An recursive process was used to solve the resulting global matrices until convergence was reached, namely when $|u_{i+1} - u_i| < 10^{-6}$.

Skin friction, Nusselt number and Sherwood number

The τ(Skin friction) is evaluated using the formula $\tau = \left(\frac{du}{d\eta}\right)_{\eta=1,1+s}$.

The rate of heat transfer (Nu) is evaluated using the formula $Nu = -\left(\frac{d\theta}{d\eta}\right)_{\eta=1,1+s}$.

The rate of mass transfer (Sh) is evaluated using the formula $Sh = -\left(\frac{dC}{d\eta}\right)_{\eta=1,1+s}$

Comparison

In absence of exothermic chemical reaction (Q_1=0) the results are good agreement with Siva Shankara Rao[36] (Tables 2).

Table 2 — Numerical comparison of results for different parameters

Parameters		MoS_2 – Water		Mono nanofluid (MoS_2 – Water)	
		Siva Shankara Rao[36]		Present values	
		Nu(1)	Sh(1)	Nu(1)	Sh(1)
Rd	2.5	1.001542	2.39315	1.001540	2.39316
	4.5	0.999984	2.38091	0.999986	2.38093
	6.5	0.999937	2.38032	0.999935	2.38034
Ec	2.1	1.001542	2.39315	1.001543	2.39317
	4.1	0.999983	2.38092	0.999984	2.38090
	6.1	0.999821	2.38087	0.999826	2.38088
B	0.2	1.001542	2.39315	1.001545	2.39314
	0.4	0.999999	2.37996	0.999998	2.37998
	0.6	0.999982	2.37881	0.999998	2.37879
Pr	0.71	1.000154	2.39315	1.000156	2.39313
	1.71	0.999984	2.38088	0.999986	2.38087
	3.71	0.999979	2.38082	0.999981	2.38080

Results and discussion

We investigate the effects of the reaction rate parameter (Q_1), activation energy (E_1), variable viscosity (B), and a non-uniform heat source on non-Darcy convective heat and mass transfer of a water-based hybrid nanofluid (MoS_2 + SiO_2/H_2O) through a porous medium within a cylindrical annulus. The coupled nonlinear governing equations are solved using the Finite Element Technique (FET) combined with Quadratic Interpolation Functions (QIF). Figures **(***2a–2c***)** through **(***17a-17c***)** illustrate the influence of various dimensionless parameters on the

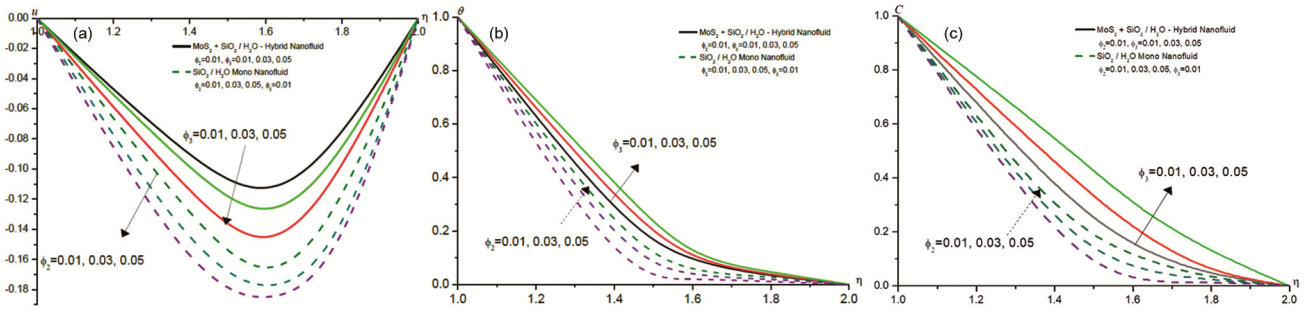

Fig. 2 — (a) Stimulus of ϕ on u; (b) Stimulus of ϕ on θ; and (c) Stimulus of ϕ on C

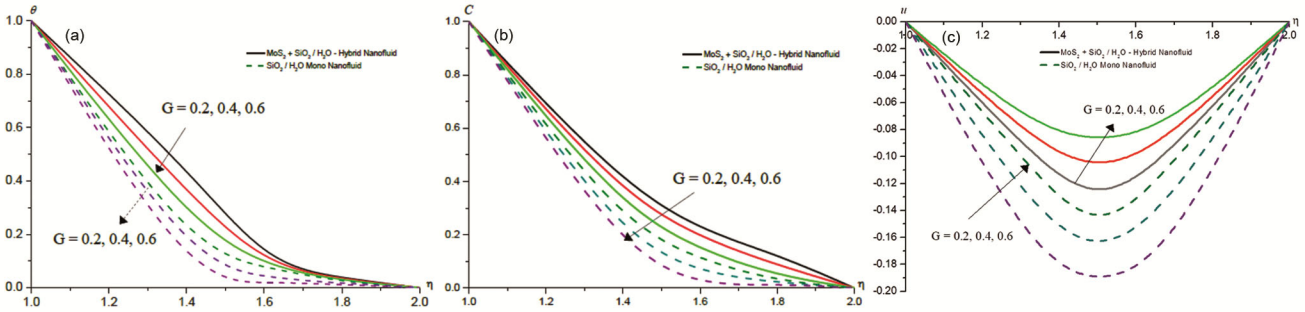

Fig. 3 — (a) Impression of G on u; (b) Impression of G on θ; and (c) Impression of G on C

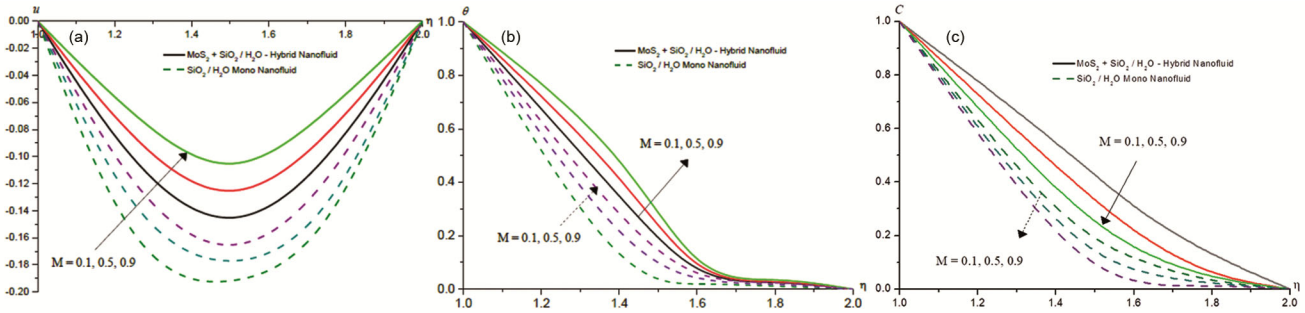

Fig. 4 — (a) Effect of M on u; (b) Effect of M on θ; and (c) Effect of M on C

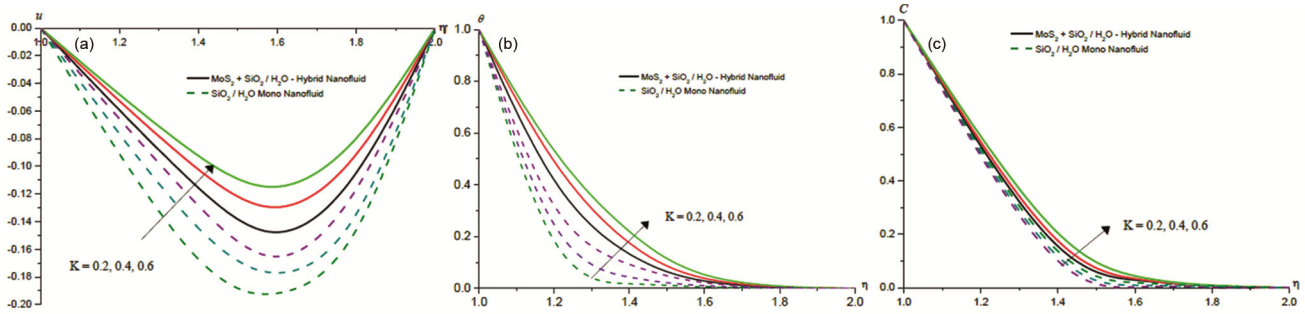

Fig. 5 — (a) Effect of K on u; (b) Effect of K on θ; and (c) Effect of K on C

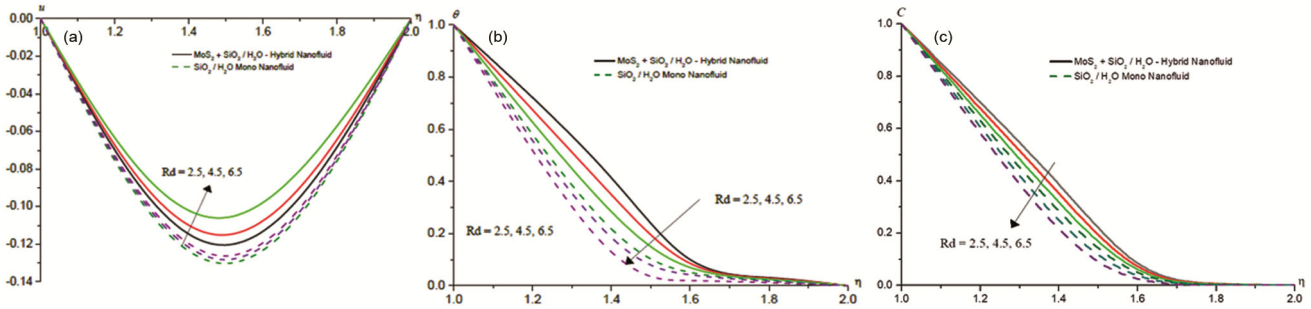

Fig. 6 — (a) Effect of Rd on u; (b) Effect of Rd on θ; and (c) Effect of Rd on C

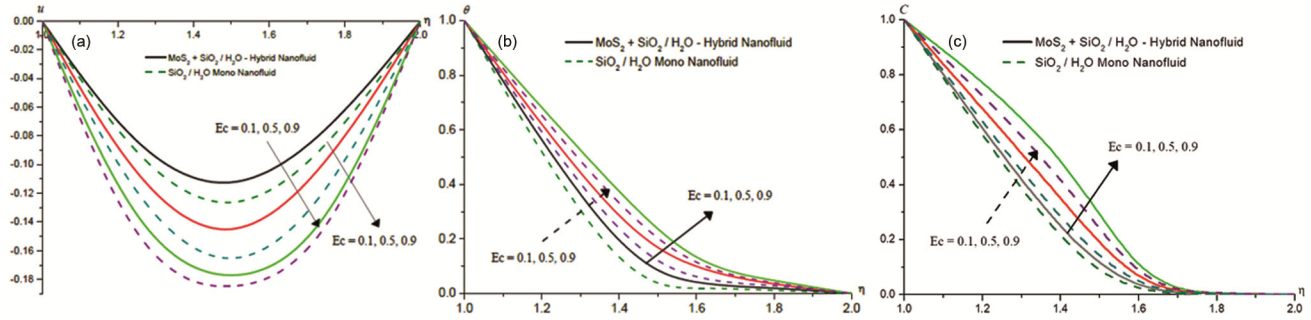

Fig. 7 — (a) Effect of con u; (b) Effect of c on θ; and (c) Effect of c on C

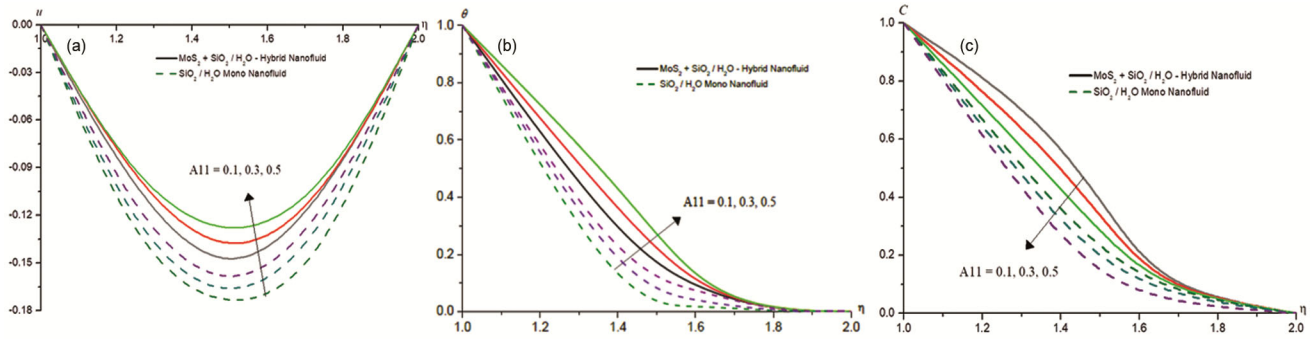

Fig. 8 — (a) Effect of A_{11} on u; (b) Effect of A_{11} on θ; and (c) Effect of A_{11} on C

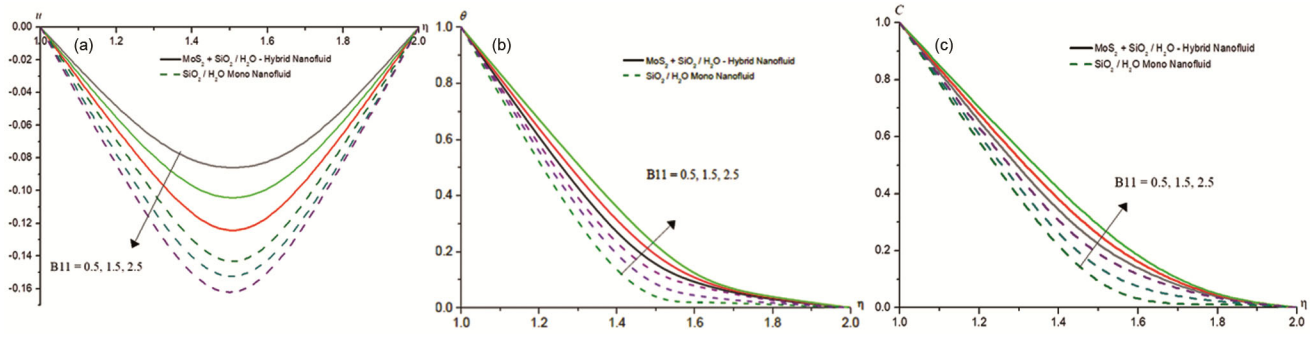

Fig. 9 — (a) Effect of B_{11} on u; (b) Effect of B_{11} on θ; and (c) Effect of B_{11} on C

velocity (*u*), temperature (θ), and nanoparticle concentration (C) distributions. The computations are carried out for the following representative parameter values: Q_1 = 0.5, Sc = 1.0, Sr = 0.5,.δ_1= 0.01,G = 0.2, M = 0.1, K = 0.2, Rd = 2.5, Ec = 0.1, A_{11} = 0.1, B_{11} = 0.5, B = 0.5, E_1 = 0.1, Pr = 6.20,ϕ= 0.1.The speed (u) goes up as the values of G/Rd/Ec/B_{11}/B/Q_1/ Pr/Sr/E_1 go up (see Figure. 3a, 6a, 7a, 9a, 10a, 11a, 12a,

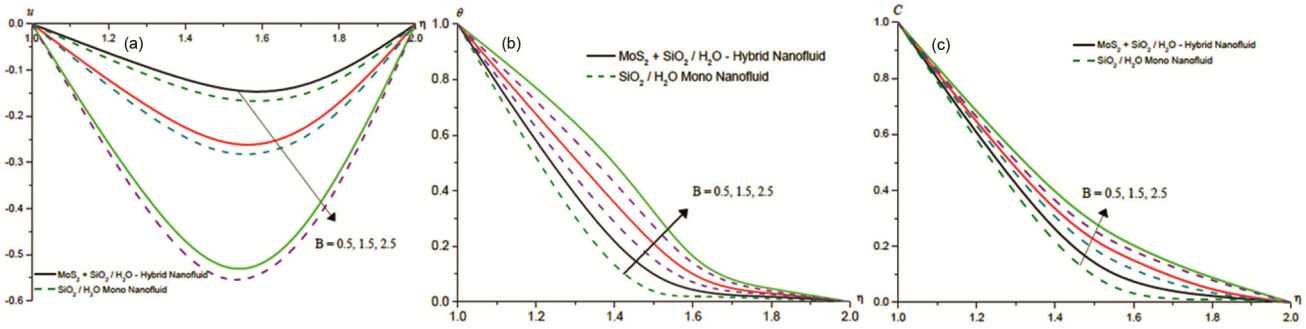

Fig. 10 — (a) Effect of B on u; (b) Effect of B on θ; and (c) Effect of B on C

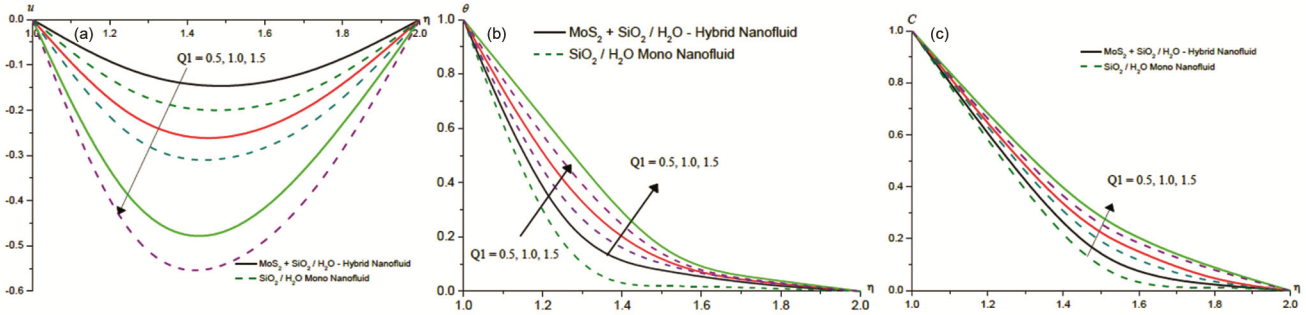

Fig. 11 — (a) Effect of Q_1 on u; (b) Effect of Q_1 on θ; and (c) Effect of Q_1 on C

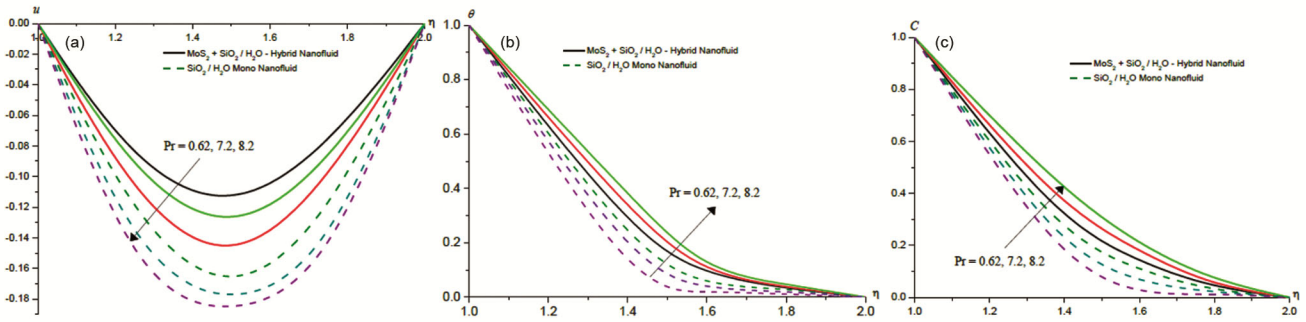

Fig. 12 — (a) Effect of Pr on u; (b) Effect of Pr on θ; and (c) Effect of Pr on C

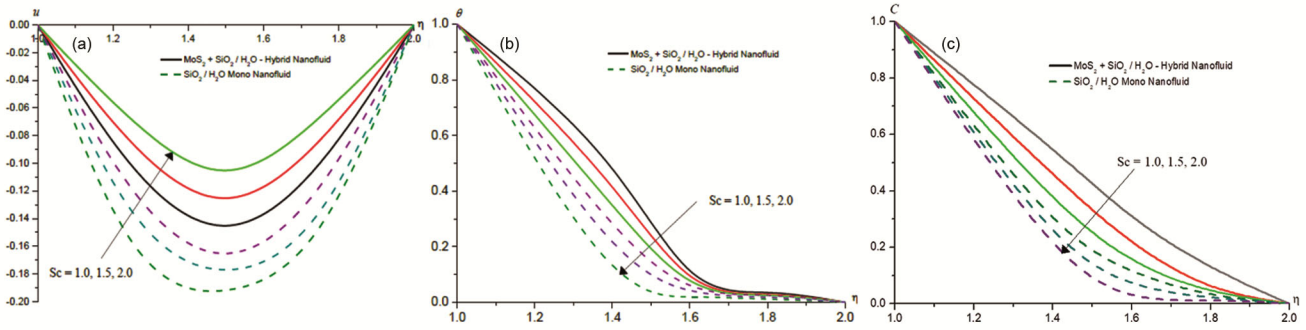

Fig. 13 — (a) Encouragement of Sc on u; (b) Encouragement of Sc on θ; and (c) Encouragement of Sc on C

14a, and 15a) in water-based hybrid and mono nanofluids. The reason for this is that as G/Rd/Ec/B_{11}/B/Q_1/Pr/Sr/E_1 numbers rise across the whole flow region, so does the thickness of the momentum boundary layer. When ϕ/M/K/A_{11}/ Sc/ Δ/δ_1 goes up (see Figure. 2a, 4a, 5a, 8a, 13a, 16a, and 17a), the velocity in the whole flow region slows down. The momentum boundary

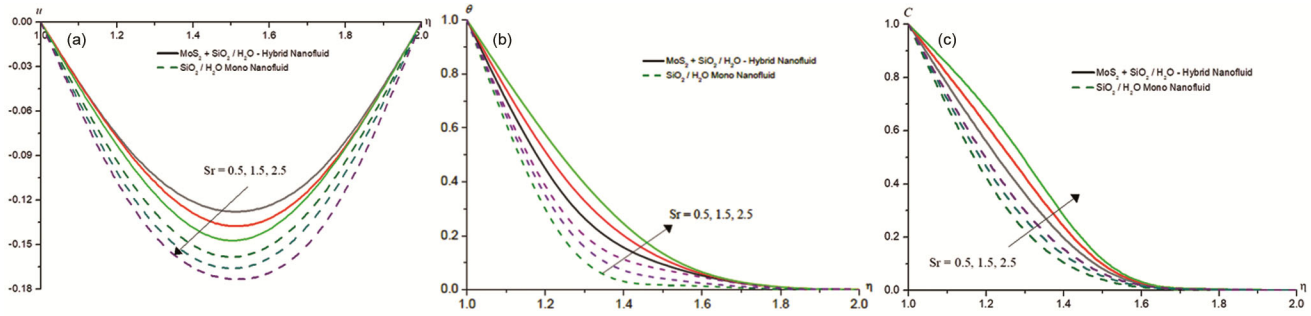

Fig. 14 — (a) Stimulus of Sr on u; (b) Stimulus of Sr on θ; and (c) Stimulus of Sr on C

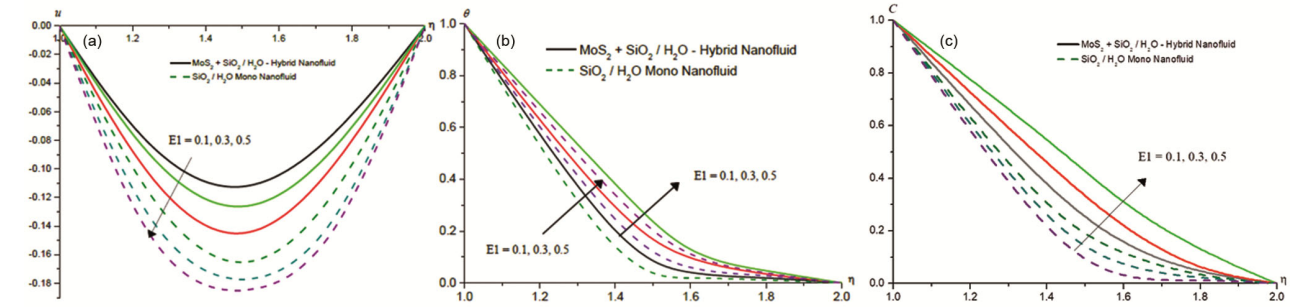

Fig. 15 — (a) Control of E_1 on u; (b) Control of E_1 on θ; and (c) Control of E_1 on C

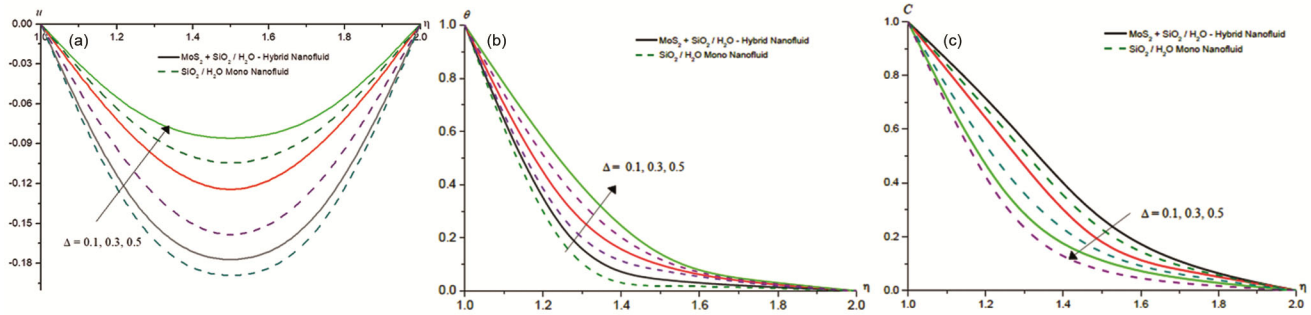

Fig. 16 — (a) Impression of Δ on u; (b) Impression of Δ on θ; and (c) Impression of Δ on C

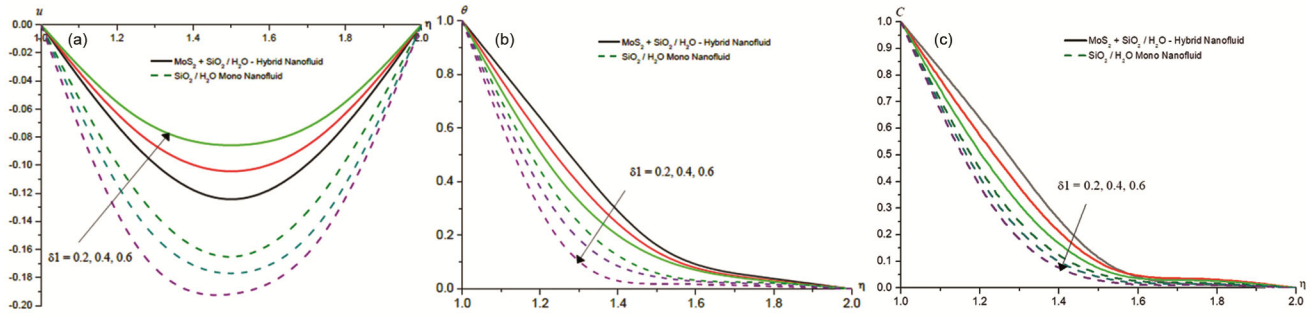

Fig. 17 — (a) Effect of δ_1 on u; (b) Effect of δ_1 on θ; and (c) Effect of δ_1 on C

layer gets thinner as $\phi/M/K/A_{11}/Sc/\Delta/\delta_1$ goes up in both nanofluids, which fits with what happened. Also, it has been seen that the size of in a mixed nanofluid is smaller than in a monofluid for all of these factors.

In hybrid nanofluid are higher than those in mono nanofluid for all parameters. In water-based hybrid/ mono nanofluids, exothermic reaction parmeter (Q_1) increases flow *u*, θ, and Φ. The temperature distribution (θ) upsurges of the values of δ/Δ

/M/K/Ec/A_{11}/B_{11}/B/Q_1/Pr/Sr /E_1 and thins with G/Rd/Ec/Sc/ϕ (see Figure. 3b, 6b, 7b) across the flow region. The thermal boundary layer thickens with δ/Δ/M/K/Ec/A_{11}/B_{11}/B/Q_1//Pr/Sr /E_1 (see Figures. 2b, 4b, 5b, 7b, 8b, 9b, 10b, 11b, 12b, 14b, 15b) and decreases with G/Rd/Ec/Sc/ϕ) increases in the flow region.

Higher the values of ϕ/Ec/B_{11}/B/Q_1/Pr/Sr /E_1 (Figure. 2c, 7c, 9c, 10c, 11c, 12c, 14c, 15c) larger the nano-concentration (C) in entire flow region while reverse effect is noticed with remaining parameters G/M/Rd/A_{11}/Sc/Δ/δ_1 (Figure. 3c, 4c, 6c, 8c, 13c, 16c, 17c). This is due to the fact that the thickness of thermal boundary layer grows with increase in ϕ/Ec/B_{11}/B/Q_1/Pr/Sr /E_1 and decays with G/Rd/A_{11}/Sc/Δ/δ_1 in water based hybrid/mono nanofluids. Because of these differences, it is clear which the measurements of C in mixed nanofluid are higher than those in mono nanofluid.

The skin friction (τ), rate of heat transfer (Nusselt number (Nu)) and rate of mass transfer (Sherwood number (Sh)) are presented (Tables 3 & 4).

Table 3 — τ (Skin friction), Nu (Nusselt number) & Sh (Sherwood number) at η = 1

Parameter		Hybrid nanofluid			Mono nanofluid		
		τ(1)	Nu(1)	Sh(1)	τ(1)	Nu(1)	Sh(1)
ϕ	0.01	-0.693949	0.951937	1.65978	-0.693966	0.951538	1.65874
	0.03	-0.693939	0.951747	1.65963	-0.694868	0.953651	1.65893
	0.05	-0.693934	0.950768	1.65958	-0.697779	0.950688	1.65905
G	0.2	-0.693949	0.957937	1.65898	-0.643966	0.954538	1.65874
	0.4	-0.681624	0.958213	1.65996	-0.681671	0.955822	1.65972
	0.6	-0.669261	0.959485	1.66066	-0.699383	0.956101	1.66041
M	0.1	-0.693949	0.951937	1.65878	-0.693966	0.950538	1.65874
	0.5	-0.692219	0.951967	1.65897	-0.692222	0.950576	1.65893
	0.9	-0.688018	0.952042	1.65937	-0.688193	0.950668	1.65937
K	0.2	-0.693949	0.952937	1.65898	-0.693966	0.952538	1.65873
	0.4	-0.693449	0.952945	1.65899	-0.693453	0.952547	1.65874
	0.6	-0.692677	0.952957	1.65969	-0.692866	0.952562	1.65875
Rd	2.5	-0.693949	0.952937	1.65892	-0.693966	0.952538	1.65874
	4.5	-0.693075	0.971732	1.66076	-0.693105	0.971103	1.66074
	6.5	-0.692688	0.979961	1.66138	-0.692724	0.979232	1.66132
Ec	0.1	-0.693949	0.952937	1.65898	-0.693966	0.952538	1.65874
	0.5	-0.694892	0.925138	1.65489	-0.694916	0.924462	1.65484
	0.9	-0.695836	0.896296	1.64796	-0.695872	0.896249	1.64793
A_{11}	0.1	-0.693949	0.952937	1.65878	-0.693966	0.952538	1.65874
	0.3	-0.693795	0.955482	1.65998	-0.693811	0.955107	1.65903
	0.5	-0.693641	0.957721	1.66026	-0.693655	0.957675	1.65931
B_{11}	0.5	-0.693949	0.952937	1.65968	-0.693966	0.952538	1.65874
	1.5	-0.697296	0.873292	1.64193	-0.697346	0.873105	1.64182
	2.5	-0.700818	0.792008	1.60903	-0.700904	0.790979	1.60844
B	0.5	-0.693949	0.952937	1.65878	-0.693966	0.952538	1.65874
	1.5	-1.456191	0.882623	1.59383	-1.456332	0.882481	1.59377
	2.5	-3.364134	0.718347	1.39628	-3.366873	0.716212	1.39457
E_1	0.1	-0.693949	0.952937	1.65888	-0.693966	0.952538	1.65874
	0.3	-0.693987	0.952263	1.55334	-0.694005	0.951857	1.55329
	0.5	-0.693999	0.952061	1.52123	-0.694016	0.951653	1.52118
Q_1	0.25	-0.693949	0.952937	1.65878	-0.693966	0.952538	1.65874
	0.50	-0.692249	0.951237	1.64998	-0.694466	0.953568	1.66374
	1.00	-0.691249	0.950737	1.63788	-0.695566	0.954538	1.67274
Pr	0.62	-0.693949	0.952937	1.65888	-0.693966	0.952538	1.65874
	7.2	-0.694824	0.937953	1.65676	-0.694846	0.937385	1.65671
	8.2	-0.695694	0.922925	1.65419	-0.695734	0.922193	1.65412
Δ	0.1	-0.663949	0.952937	1.65878	-0.663966	0.952538	1.65874
	0.3	-0.668998	0.951512	1.65488	-0.669114	0.951129	1.65473
	0.5	-0.674103	0.950967	1.65276	-0.674318	0.950714	1.65273
δ_1	0.2	-0.693949	0.952937	1.65878	-0.693966	0.952538	1.65874
	0.4	-0.693941	0.953084	1.68632	-0.693958	0.952687	1.68627
	0.6	-0.693934	0.954218	1.71152	-0.693951	0.952823	1.71146

Table 4 — τ (Skin friction), Nu (Nusselt number) & Sh (Sherwood number) at η = 2

Parameter		Hybrid nanofluid			Mono nanofluid		
		τ(2)	Nu(2)	Sh(2)	τ(2)	Nu(2)	Sh(2)
ϕ	0.01	0.590163	1.00794	0.584974	0.590143	1.00698	0.585001
	0.03	0.590186	1.00888	0.584949	0.590096	1.00727	0.584884
	0.05	0.590212	1.00981	0.584927	0.590053	1.00754	0.584778
G	0.2	0.590163	1.00794	0.584974	0.590143	1.00698	0.585001
	0.4	0.584983	1.00693	0.584464	0.584985	1.00597	0.584495
	0.6	0.579814	1.00592	0.583957	0.579835	1.00496	0.583991
M	0.1	0.590163	1.00794	0.584974	0.590143	1.00698	0.585001
	0.5	0.588682	1.00794	0.584862	0.588623	1.00693	0.584884
	0.9	0.585256	1.00782	0.584595	0.585109	1.00682	0.584612
K	0.2	0.590963	1.00794	0.584974	0.590943	1.00698	0.585051
	0.4	0.590821	1.00792	0.584954	0.590815	1.00503	0.585041
	0.6	0.590535	1.00703	0.584014	0.590549	1.00407	0.585023
Rd	2.5	0.590163	1.00794	0.584974	0.590143	1.00698	0.585001
	4.5	0.589523	1.00507	0.583856	0.589515	1.00448	0.583867
	6.5	0.589236	1.00372	0.583524	0.589235	1.00329	0.583532
Ec	0.1	0.590163	1.00794	0.584974	0.590143	1.00698	0.585001
	0.5	0.591041	1.03952	0.584784	0.591029	1.03883	0.584747
	0.9	0.591924	1.07121	0.587849	0.591921	1.07083	0.587813
A_{11}	0.1	0.590163	1.00794	0.584974	0.590143	1.00698	0.585001
	0.3	0.590026	1.00567	0.584879	0.590004	1.00469	0.584908
	0.5	0.589888	1.00342	0.584794	0.589865	1.00243	0.584825
B_{11}	0.5	0.590163	1.00794	0.584974	0.590143	1.00698	0.585001
	1.5	0.592804	1.04541	0.588747	0.592809	1.04477	0.588789
	2.5	0.595594	1.08499	0.596004	0.595627	1.08471	0.596127
B	0.5	0.590163	1.00794	0.584974	0.590143	1.00698	0.585001
	1.5	0.894919	1.06792	0.618238	0.894949	1.06754	0.618263
	2.5	1.556175	1.21476	0.717758	1.557723	1.21595	0.718437
Q_1	0.25	0.590163	1.00794	0.584974	0.590143	1.00698	0.585001
	0.50	0.590154	1.00789	0.584966	0.590145	1.00701	0.585006
	1.00	0.590145	1.00778	0.584959	0.590149	1.00712	0.585012
E_1	0.1	0.590163	1.00794	0.584974	0.590143	1.00698	0.585001
	0.3	0.590196	1.00843	0.616405	0.590175	1.00748	0.616432
	0.5	0.590205	1.00858	0.625636	0.590185	1.00763	0.625662
Pr	0.62	0.590163	1.00794	0.584974	0.590143	1.00698	0.585001
	7.2	0.590942	1.02167	0.585572	0.590929	1.02084	0.585586
	8.2	0.591724	1.03546	0.586488	0.591719	1.03477	0.586512
Δ	0.1	0.590163	1.00794	0.584974	0.590143	1.00698	0.585001
	0.3	0.579814	1.00591	0.583949	0.579836	1.00494	0.583983
	0.5	0.569476	1.00389	0.582934	0.569547	1.00292	0.582974
δ_1	0.2	0.590163	1.00794	0.584974	0.590143	1.00698	0.585001
	0.4	0.590157	1.00784	0.579577	0.590136	1.00688	0.579606
	0.6	0.590151	1.00775	0.574663	0.590134	1.00679	0.574694

The augmentation in G, M, K, Rd, and δ_1 increases Nu and Sh at the inner cylinder (η=1) but decreases them at the outer cylinder (η=2) for both water-based hybrid and mono nanofluids. A higher reaction rate (Q_1) results in lower τ, Nu, and Sh in the hybrid nanofluid, while these parameters are higher in the mono nanofluid at η=1; however, the reverse trend is observed at η=2. An increase in B_{11}, Ec, B, E_1, or Pr enhances τ but reduces Nu and Sh at η=1, whereas at η=2, τ, Nu, and Sh increase in both water-based hybrid and mono nanofluids.An increase in the temperature difference ratio (δ_1) leads to a smaller τ and larger Nu and Sh at η=1, while at η=2, τ, Nu, and Sh decrease for both types of nanofluids. The augmentation in nanoparticle volume fraction (ϕ) reduces τ at η=1 but increases it at η=2 in both hybrid

and mono nanofluids. Nu and Sh decrease in the hybrid nanofluid and increase in the mono nanofluid at η=1; however, at η=2, Nu increases and Sh decreases in both hybrid and mono nanofluids with a rise in ϕ.

It is evident from the above discussion that Nu and Sh are higher in water-based hybrid nanofluids compared to water-based mono nanofluids.

Conclusion

This investigation examines how exothermic chemical reaction (Q_1), variable viscosity (B), activation energy (E_1), and thermal radiation (Rd) affect hydro magnetic convective heat transfer flow of water-based hybrid nanofluid. Coupled nonlinear governing equations were numerically solved by applying Finite Element Technique with quadratic interpolation functions. The key outcomes are:

- Increasing in G/Rd/Ec/B_{11}/B/Q_1/Pr/Sr /E_1 upsurges velocity in water based hybrid/mono nanofluids in the flow region while reverse effect is seen with the higher values of ϕ/M/K/A_{11}/Sc/Δ/δ_1.
- Increasing in ϕ/Ec/B_{11}/B/Q_1/Pr/Sr/E_1 enhances both θ& C in hybrid/mono nanofluids while increasing in G/Rd/Sc /Δ/δ_1 exhibits depreciation tendency in θ & C.
- The shear stress τ enhances at η = 1 and reduces at η = 2 with the rising values of G/M/Rd/ A_{11}/δ_1 while reverse effect is observed in τ with the larger values of Ec/B_{11}/B/E_1/Pr in hybrid/mono nanofluids. Also skin friction τ reduces at both the cylinders with the larger values of Δ.
- The values of τ at η = 1 &2 in water based hybrid nanofluid are relatively greater than those in mono nanofluid.
- The rate of heat transfer (Nu) augmentss at η = 1 &2 with increasing K in both nanofluids.
- Decreasing ϕ/Ec/ B_{11}/ B/ E_1/ Pr enhances Nu at η = 1 and decays at η = 2 in both nanofluids. Reverse effect is observed in case of G/ M/ Rd/ A_{11}/δ_1.
- For increasing in Δ Nu reduces at both the cylinders in water based hybrid/mono nanofluids.
- Rate of mass transfer (Sh) boosts up at η = 1 and declines at η = 2 for the higher values of G/ M/ Rd/ A_{11}/$\delta_1$while effect is observed with the increasing values of Ec/ B_{11}/ B/ E_1/ Pr.
- Sh experiences depreciation at η = 1 & 2 for the higher values of Δ.
- τ, Nu and Sh reduces in hybrid and enhances in mono nanofluid at both the cylinders with higher values of reaction rate(Q_1).
- The variations of Nu and Sh for different parameters show that rates of heat and mass transfer in hybrid nanofluid are relatively greater than those in mono nanofluid.

Nomenclature:

	Description	SI Unit
T	*Fluid temperature*	*Kelvin (K)*
u	*Axial velocity in porous media*	ms^{-1}
ρ	*Fluid density*	kgm^{-3}
C_p	*Specific heat capacity*	$Jkg^{-1}K^{-1}$
ν	*Kinematic viscosity*	m^2s^{-1}
C	*Fluid concentration*	$mol\ L^{-1}$
μ	*Dynamic viscosity*	pas^{-1}
k	*Thermal conductivity*	$Wm^{-1}K^{-1}$
K_T	*Mass diffusion coefficient*	m^2s^{-1}
β	*Thermal expansion Coefficient*	K^{-1}
Pr	*Prandtl number*	*Dimensionless*
g	*Acceleration due to gravity*	ms^{-2}
σ	*Electrical Conductivity*	Sm^{-1}
σ^*	*Stefan Boltzmann constant*	$Wm^{-2}K^{-4}$
k	*permeability of the porous medium*	m^2
Q_1'	*heat absorption*	$J\ K^{-1}\ m^{-3}\ s^{-1}$

Acknowledgement

The author wishes to express sincere thanks to the honourable referees for the valuable comments and suggestions to improve the quality of the paper

Conflict of interest

All authors declare no conflict of interest.

References

1 Choi SUS & Eastman JA, Enhancing thermal conductivity of fluids with nanoparticles. *Argonne National Lab*, *DuPage County*, *IL, USA*, (1995).

2 Muhammad NM & Sidik NAC, Applications of Nanofluids and Various Mini channel Configurations for Heat Transfer Improvement: A Review of Numerical Study. *J Adv Res Fluid Mech Therm Sci*, 46 (2018) 49.

3 Husam AH, Zainab A & Sopian K, Heat Transfer Enhancement Using Nanofluids for Cooling A Central Processing Unit (CPU) System. *J Adv Res Fluid Mech Therm Sci*, 51 (2018) 145.

4 Liu J & Deng ZS, Nano-cryosurgery: advances and challenges. *J Nanosci Nanotechnol*, 9 (2009) 4521.

5 Yaseen M, Rawat SK & Kumar M, Hybrid nanofluid (MoS_2–SiO_2/water) flow with viscous dissipation and Ohmic heating on an irregular variably thick convex/concave-shaped sheet in a porous medium. *Heat Transfer*, 51 (2022) 789.

6 Mishra A & Pathak G, A comparative analysis of MoS_2-SiO_2/H_2O hybrid nanofluid and MoS_2-SiO_2-GO/H_2O ternary hybrid nanofluid over an inclined cylinder with heat generation/absorption. *Numer Heat Transf A*, 85 (2023) 2724.

7 Iqbal Z, Maraj EN, Ehtsham Azhar & Zaffar Mehmood, A novel development of hybrid (MoS_2− SiO_2/H_2O) nanofluidic curvilinear transport and consequences for effectiveness of shape factors. *J Taiwan Inst Chem Eng*, 81 (2017) 150.

8 Patil P, Goudar B & Sheremet MA, Tangent hyperbolic ternary hybrid nanofluid flow over a rough-yawed cylinder due to impulsive motion. *J Taibah Univ Sci*, 17 (2023) 2199664.

9 Patil P, Shashikant A & Hiremath P, Effects of surface roughness on mixed convection nanoliquid flow over slender cylinder with liquid hydrogen diffusion. *Int J Hydrogen Energy*, 44 (2019) 11121.

10 Liu D, Song YZ, Sun SL, Yang S, Ahmed B & Muhammad T, Heat transfer performance and entropy generation analysis of Taylor–Couette flow with helical slit wall. *Case Stud Therm Eng*, 53 (2024) 103852.

11 Hanif H, Lund LA & Shafie S, Dynamics of Ag–TiO_2 /H_2O between two coaxial cylinders: a computational approach. *Eur Phys J Plus*, 138 (2023) 1.

12 Sun SL, Liu D, Wang YZ, Qi YL & Kim HB, Convective heat transfer and entropy generation evaluation in the Taylor–Couette flow under the magnetic field. *Int J Mech Sci* 252 (2023) 108373.

13 Zangooee M, Hosseinzadeh K & Ganji DD, Hydrothermal analysis of Ag and CuO hybrid NPs suspended in mixture of water 20%+ EG 80% between two concentric cylinders. *Case Stud Therm Eng*, 50 (2023) 103398.

14 Hafez N, EHD peristaltic flow of sisko fluid under the effects of convection and endoscope. *Ain Shams Eng J*, (2024) 102647.

15 Swamy HK, Reddy NK, Sankar M & Peddinti PR, Conjugate heat transfer of aqueous hybrid nanoliquid between coaxial cylinders subjected to magnetic field. *Int J Thermofluids* 17 (2023) 100299.

16 Mahfoud B, Stability of flowing PbLi alloy between coaxial cylinders under magnetic field. *Algerian J Eng Technol*, 8 (2023) 322.

17 Hanif H, Ilias MR, Iqbal Z, Shafie S, Sharifah EA & Alqarni MM, Heat transfer in hybrid nanofluid flow between two coaxial cylinders. *Case Stud Therm Eng*, 59 (2024) 104327.

18 Shaiq S, Maraj EN & Iqbal Z., Remarkable role of C 3 H 8 O 2 on transportation of MoS 2 /SiO 2 hybrid nanoparticles influenced by thermal deposition and internal heat generation. *J Phys Chem Solids*, 126 (2019) 294.

19 Krishna MV, Ahamad NA & Chamkha AJ, Hall and ion slip impacts on unsteady MHD convective rotating flow of heat generating/absorbing second grade fluid. *Alex Eng J*, 60 (2021).

20 Roy N & Pal D, Influence of Activation Energy and Nonlinear Thermal Radiation with Ohmic Dissipation on Heat and Mass Transfer of a Casson Nanofluid Over Stretching Sheet. *J Nanofluids*, 11 (2022) 819.

21 Martins OA, Adebayo AO, Adeosun AT, Akindele AO, Oladapo OA, Olajide OA & Peter A, Significance of variable electrical conductivity on non-Newtonian fluid flow between two vertical plates in the coexistence of Arrhenius energy and exothermic chemical reaction. *Partial Diff Equ Appl Math*, 4 (2021) 100184.

22 Obalalu AM, Ajala AO, Akindele AO, Oladapo OA, Adepoju O & Jimoh OM, Unsteady squeezed flow and heat transfer of dissipative casson fluid using optimal homotopy analysis method: An application of solar radiation. *Partial Diff Equ Appl Math*, 4 (2021) 100146.

23 Obalalu AM, Ajala OA, Abdulraheem A & Oladimeji AA. The influence of variable electrical conductivity on non-Darcian Casson nanofluid flow with first and second-order slip conditions. *Partial Diff Equ Appl Math*, (2021) 100084.

24 Adeshina T Adeosun & Joel C Ukaegbu, Effect of the variable electrical conductivity on the thermal stability of the MHD reactive squeezed fluid flow through a channel by a spectral collocation approach. *Partial Diff Equ Appl Math*, 5 (2022) 100256.

25 Babu DC, Influence of Activation Energy, Variable viscosity, partial slip on MHD mixed convective Heat Transfer flow of Nanofluid past Stretching Surface with Newtonian Cooling. *Int J Comput Appl*, 185 (2023) 54.

26 Sreedevi G, Prasada Rao DRV & Ali J Chamka, Convective heat transfer of a nano fluid over a stretching sheet with variable viscosity and hall effect. *J Math Fluid Mech*, 3 (2020) 1023.

27 Nagasasikala M, Impact of Exothermic reaction associated with activation energy on MHD rotating convective heat and mass transafer flow of Water/Eg/Eo based TiO_2 nanofluid past a stretching surface with variable viscosity. *J Eng Comput Archit*, 15 (2025) 12.

28 Forchheimer P, Wsserbewegungdurch Boden. 45th Edition, Zeitschrift des Vereins Deutscher Ingenieure, Dusseldorf, (1901).

29 Wooding R, Steady State Free Thermal Convection of Liquid in a Saturated Permeable Medium. *J Fluid Mech*, 2 (1957) 273.

30 Brinkman HC, A Calculation of the Viscous Force Exerted by a Flowing Fluid on a Dense Swarm of Particles. *Appl Sci Res*, 1 (1947) 27.

31 Brinkman HC, On the Permeability of Media Consisting of Closely Packed Porous Particles. *Appl Sci Res*, 1 (1947) 81.

32 Ali A, Pasha AA, Tirth V, Sarfraz MM, Algahtani A & Irshad K, Thermal analysis of MHD radiative flow of hybrid nanofluids in a porous medium between coaxial cylinders. *J Radiat Res Appl Sci*, 18 (2025) 101699.

33 Nield DA & Bejan A, Convection in porous media. *Springer International publishing AG*, *Berlin*, 2017.

34 Usman M, Hamid M, Zubair T, Ul Haq R & Wang W, Cu-Al_2O_3/Water hybrid nanofluid through a permeable surface in the presence of nonlinear radiation and variable thermal conductivity *via* LSM. *Int J Heat Mass Transfer*, 126 (2018) 1347.

35 Oztop H F & Abu-Nada E, Numerical study of natural convection in partially heated rectangular enclosures filled with nanofluids. *Int J Heat Fluid Flow*, 5 (2008) 1326.

36 Rao JSS, Hydromagnetic non-darcy convective heat transfer flow of Eg-based MoS_2 – SiO_2 nano fluids in cylindrical annulus with heat sources and activation energy–a finite element approach. *Ganita*, 75 (2025) 21.